NUMERICAL SOLUTION OF BIO-NANO-CONVECTION TRANSPORT FROM A HORIZONTAL PLATE WITH BLOWING AND MULTIPLE SLIP EFFECTS

Md. Jashim Uddin
Mathematics Dept., Faculty of Science and Technology, American International University-Bangladesh, Kuril, Dhaka 1229, Bangladesh. Email: jashim_74@yahoo.com
M.N. Kabir*
Faculty of Computer Systems and Software Engineering, University Malaysia Pahang, 26300 Gambang, Pahang, Malaysia. Email: nomanikabir@ump.edu.my
Yasser Alginahi
Department of Computer Science, Taibah University, P.O. Box 344, Madinah, Saudi Arabia. Email: yginahi@taibahu.edu.sa
O. Anwar Bég
Fluid Mechanics and Bio-Propulsion, Aeronautical and Mechanical Engineering Department, University of Salford, M54WT, UK. Email:O.A.Beg@salford.ac.uk and gortoab@gmail.com

*Corresponding Author-email: nomanikabir@ump.edu.my, Phone: +060109154807

Numerical Solution of Bio-nano-convection transport from a horizontal plate with Blowing and Multiple Slip Effects

Abstract

In this paper, a new bio-nano-transport model is presented. The effects of first and second order velocity slips, thermal slip, mass slip, and gyro-tactic (torque-responsive) microorganism slip of bioconvective nanofluid flow from a moving plate under blowing phenomenon are numerically examined. The flow model is expressed by partial differential equations which are converted to a similar boundary value problem by similarity transformations. The boundary value problem is converted to a system of nonlinear equations which are then solved by a Matlab nonlinear equation solver *fsolve* integrated with a Matlab ODE solver *ode15s*. The effects of selected control parameters (first order slip, second order slip, thermal slip, microorganism slip, blowing, nanofluid parameters) on the non-dimensional velocity, temperature, nanoparticle volume fraction, density of motile micro-organism, skin friction coefficient, heat transfer rate, mass flux of nanoparticles and mass flux of microorganisms are analyzed. Our analysis reveals that a higher blowing parameter enhances micro-organism propulsion, flow velocity and nano-particle concentration, and increases the associated boundary layer thicknesses. A higher wall slip parameter enhances mass transfer and accelerates the flow. The MATLAB computations have been rigorously validated with the second-order accurate finite difference Nakamura tri-diagonal method. The current study is relevant to microbial fuel cell technologies which combine nanofluid transport, bioconvection phenomena and furthermore finds applications in nano-biomaterials sheet processing systems.

Keywords: *Bioconvection; motile micro-organism propulsion; Second-order velocity slip, nanofluids; boundary layers; nano-bio green fuel cells; numerical solutions.*

NOMENCLATURE

a, b first and second order velocity slip parameter (-)

$\tilde{b}$ chemotaxis constant (m)

c thermal slip parameter (-)

C nanoparticle volume fraction (-)

d mass slip parameter (-)

D_1 variable thermal slip factor (m)

$(D_1)_0$ constant thermal slip factor (m)

D_B Brownian diffusion coefficient ($m^2 s^{-1}$)

D_n diffusivity of microorganisms ($m^2 s^{-1}$)

D_T thermophoretic diffusion coefficient ($m^2 s^{-1}$)

e microorganism slip parameter (-)

E_1 variable mass slip factor (m)

$(E_1)_0$ constant mass slip factor (m)

F_1 variable microorganism slip factor (m)

$(F_1)_0$ constant microorganism slip factor (m)

$f(\eta)$ dimensionless stream function (-)

g acceleration due to gravity (ms^{-2})

h dimensionless pressure (-)

$\bar{j}$ vector flux of microorganism (kgm^{-2} s^{-1})

k thermal conductivity (Wm^{-1}K^{-1})

L characteristic length (m)

Lb bioconvection Lewis number (-)

Le Lewis number (-)

n volume fraction of motile microorganisms (-)

N_1 variable first order velocity slip factor (sm^{-1})

$(N_1)_0$ constant first order velocity slip factor (sm^{-1})

N_2 variable second order velocity slip factor (sm^{-1})

$(N_1)_0$ constant second order velocity slip factor (sm^{-1})

Nb Brownian motion parameter (-)

$Nn_{\bar{x}}$ local density number of the motile microorganisms (-)

Nt thermophoresis parameter (-)

Nr buoyancy ratio parameter (-)

$Nu_{\bar{x}}$ local Nusselt number (-)

Pe bioconvection Péclet number (-)

Pr Prandtl number (-)

$\bar{p}$ pressure (Pa)

q_m wall mass flux (ms^{-1})

q_n wall motile microorganisms flux (ms^{-1})

q_w wall heat flux (Wm^{-2})

Ra Rayleigh number (-)

$Ra_{\bar{x}}$ local Rayleigh number (-)

Rb bioconvection Rayleigh number (-)

s Stefan blowing parameter (-)

$Sh_{\bar{x}}$ local Sherwood number (-)

T nanofluid temperature (K)

$\bar{u}, \bar{v}$ velocity components along $\bar{x}-$ and $\bar{y}-$ axes (ms^{-1})

U_r reference velocity (ms^{-1})

$\bar{u}_w$ velocity of the plate (ms^{-1})

$\tilde{\bar{u}}, \tilde{\bar{v}}$ average directional swimming velocity of microorganisms along the axes (ms^{-1})

W_c constant maximum cell swimming speed (ms^{-1})

$\bar{x}, \bar{y}$ Cartesian coordinates ($\bar{x}$ − axis is aligned along and $\bar{y}$ − axis is normal to the plate) (m)

Greek symbols

α effective thermal diffusivity (m^{2}s^{-1})

β volumetric expansion coefficient of nanofluid (K^{-1})

γ density of motile microorganisms (kg m^{-3})

δ_C nano-particle concentration boundary layer

δ_m momentum boundary layer

δ_n micro-organism concentration boundary layer

δ_T thermal boundary layer

η similarity variable (-)

$\theta(\eta)$ dimensionless temperature (-)

μ dynamic viscosity of the fluid ((Nsm^{-2}))

ν kinematic viscosity of the fluid (m^2 s^{-1})

ρ_f fluid density (kg m^{-3})

ρ_p nanoparticle mass density (kg m^{-3})

$(\rho c)_f$ heat capacity of the fluid (J kg^{-3} K^{-1})

$(\rho c)_p$ heat capacity of the nanoparticle material (J kg^{-3} K^{-1})

τ ratio between the effective heat capacity of the nanoparticle material and heat capacity of the fluid (-)

$\phi(\eta)$ rescaled nanoparticle volume fraction (-)

$\chi(\eta)$ rescaled density of motile microorganisms (-)

ψ stream function (-)

Subscripts/superscripts

w condition at the wall

∞ free stream condition

$'$ differentiation with respect to η

1. INTRODUCTION

Nanotechnology is an emerging area of research which has stimulated considerable interest in both academia and industry in the 21st century. In this area, nano-particles suspended in conventional fluids (water, ethylene glycol, etc.) which constitute *nanofluids* have been found to have diverse applications in aggregate manufacture [1], solar collectors [2], liquid-liquid extraction columns [3], heat exchangers [4], bubble absorption technologies [5], reactors [6], refrigeration [7], microscale

mixers [**8**], coolants [**9**] and waste heat boiler systems [**10**]. Prior to the deployment of nanofluids in the applications, they require extensive laboratory and field tests and also theoretical analysis and computational simulation. Metals have over three times greater thermal conductivity than conventional heat transfer fluids. Nanofluid is a fluid comprising of two substances i.e., fluid and nanoparticles that are combined to fabricate a heat transfer medium which achieves much greater heat conductivity than the fluid itself. In the context of mathematical modelling, two thermal conductivity and fluid mechanical formulations have proven to be most popular, namely the Buongiornio model [**11**] and the Twari-Das model [**12**]. Both models fit neatly into the boundary-layer theory framework although the former features a nano-particle volume fraction conservation equation with momentum and energy equations whereas the latter generally comprises momentum and energy conservation equations only. Recent studies employing these models have incorporated a wide range of computational algorithms for the solution of the associated boundary-layer problems. Kothandapani and Prakash [13] investigated radiative-reactive peristaltic magnetic nanofluid pumping using the homotopy perturbation method, observing that nanoparticles significantly enhance temperatures. Prasad *et al.* [14] used Buonjiorno's model to study laminar natural convection from an isothermal sphere to nanofluid-saturated porous media by Keller-box method. They found that increasing thermophoresis generates a substantial increment in both fluid temperature and nano-particle concentration values whereas the nanofluid boundary layer flow is decelerated with second order porous drag while temperature and nano-particle concentration are both enhanced. Further article addressing multi-physical nanofluid flow problems have been communicated by Uddin *et al*. [**15**] (for magnetized reactive nanofluids using Maple 17 software), Prasad *et al*. [**16**] for micropolar rheological nanofluid double-diffusive convection from a cylindrical body and Rajesh *et al*. [**17**] for unsteady nanofluid dynamics from a translating curved body (using an explicit finite difference solver). Rana and Bég [**18**] studied variable nano-layer conductivity effects on inclined plane magneto-nanofluid flow by finite element method. Rashidi *et al*. [**19**] employed a differential transform algorithm to examine entropy generation (Bejan nmber) effects on steady swirling nanofluid from a permeable rotating disk in a magnetic field. Yadav et al. [**20**] address convective flowin a horizontal layer of an electrically-conducting alumina–water nanofluid for free–free, rigid–free and rigid–rigid boundaries under a magnetic field by a Galerkin approach.

Bioconvection has also emerged as an important sub-branch of thermofluid sciences in recent years [**21, 22**]. Bioconvection refers to convective phenomenon generated by the motion of motile microorganisms in a base fluid. Specifically, bioconvection occurs due to hydrodynamic instability caused by accumulation of upward swimming motile microorganisms in the upper areas of the fluid. Motile microorganisms are able to propel themselves in different surrounding environments e.g., magnetic field, light, gravity or chemical attraction. Nanoparticles do not exhibit self-propulsion mechanisms and are characterized by Brownian motion and thermophoresis. A combination of nanoparticles and motile microorganisms in a suspension therefore enables dual benefits to be exploited i.e. directional control of micro-organisms (which aids homogenous distribution) and enhancement of macroscopic thermal properties of nanofluids. Bioconvection mechanism is used to design ecological fuels e.g. bioethanol [**23**], fuel cells [**24**] and photo-bio-reactors [**25-28**]. Biomass can be efficiently produced from microalgae in bioconvection by controlling the flue gas condition and this results in more sustainable photobioreactors [**28**]. A number of micro-organism propulsion mechanisms are observed e.g., geotactic, chemo-tactic, gyro-tactic, photo-tactic, oxy-tactic and magneto-tactic which relate to physical and chemical properties of gravity, chemicals, light, oxygen, magnetism of surrounding medium. Bioconvective

fluid dynamics has also stimulated considerable attention in the mathematical modelling community. Since algae micro-organisms are potential source of biofuels in the future renewable energy (owing to their high starch/cellulose and availability in nature), numerous theoretical studies have been centered on understanding of the mechanisms inherent in bioconvection. Xu [29] examined the bioconvective nanofluid flow over a vertical wall with an external power-law stream by a *passively controlled nanofluid model*. The author evaluated the effects of Prandtl number, Grashof number, bioconvection Rayleigh number, Schimdt number, Lewis number and bioconvection Péclet number on the concentration of motile micro-organisms. Zaimi *et al.* [30] simulated energy transfer problem past a stretchable/shrinkable sheet placed in a *nanofluid* with gyrotactic microorganisms under suction. They observed that local Sherwood number, local Nusselt number, local density of the motile microorganisms and skin friction coefficient are enhanced with greater suction. Kuznetsov [31] worked on a shallow layer of nanofluid with oxytactic microorganisms where bioconvection exhibits an oscillatory mode. The authors presented approximate analytical solutions of the problem with Galerkin approach. Bég *et al.* [32] used Maple 17 software and a Chebyschev spectral algorithm to study bioconvective rheological nanofluid flow in a Darcian porous media comprising gyrotactic microorganisms in a free moving stream. Other studies were carried out by Kuznetsov [33] and Bég *et al.* [34].

In many chemical and biophysical systems, the conventional *no-slip* wall condition is violated. This phenomenon arises in many applications e.g., trickle-flow reactors [35], viscoplastic die extrusion [36], polymer melt capillary dynamics [37], biopolymeric pumping with peristaltic devices [38], magnetohydrodynamic flow of micropolar fluids [39], hydromagnetic flow of thermo-solutal nanofluids [40] and food sterilization systems [41]. The term *velocity slip* refers to the property of *non-adherence* of a certain fluid to a boundary wall. This type of slip may takes place on the wall of the geometry for the fluid containing nanoparticles e.g., biopolymers, emulsions, suspensions, certain biofuels etc. Slip also arises on hydrophobic walls in fuel cells and their analysis necessitates amendment in the boundary conditions which can be obtained by incorporating slip factors for velocity and temperature. Moreover, the species diffusing simultaneously may cause mass (solutal) slip. Some related studies of slip hydrodynamics are conducted by Wang [42] for stagnation Newtonian flows, Turkyilmazoglu [43] for magnetic nanofluid slip convection flow and Uddin *et al.* [44] for magnetohydrodynamic nanofluid flow over an extending/contracting biopolymer sheet. Moreover, Ibrahim and Shankar [45] analyzed magnetic Sakiadis nanofluid flow with wall transpiration, velocity, thermal and mass slips. Uddin *et al.* [46] investigated nanofluid slip flow in a permeable material with variable viscosity effects with g-Jitter mixed convection. Das [47] addressed nanofluid dynamics in a porous stretching sheet with a slip, temperature dependent internal heat generation and thermal buoyancy for water-based nanofluids with copper and aluminium oxides.

All previous mathematical models did not consider the normal interfacial velocity due to species (mass) diffusion. However, there are many industrial systems (e.g. paper drying processes) where species transfer occurs via evaporation. Based on the water content and the temperature of the wet paper sheet, species transfer may be significant and may produce *blowing* which is known as *Stefan blowing* since the term is originated from the Stefan problem associated with species transfer [48]. Species diffusion generates a *bulk motion* of fluid that causes an additional motion of fluid generating the blowing effect. This has been discussed in text books on heat and mass transfer [49] and on magnetohydrodynamic transport phenomena [50]. To reflect the blowing effects for large mass transfer flux via the transfer flux of species, a blowing parameter is used to provide a

correction factor [51, 52]. Species transfer depends on the flow field that is influenced by the mass blowing at the wall. All of these generate a coupling between momentum and concentration fields. Many research works have been conducted for fluid flow with blowing phenomenon. Fang and Jing [53] illustrated a flow of a viscous fluid along a stretchable sheet considering blowing effects. Uddin et al. [54] studied blowing and multiple-slip effects on a moving horizontal plate located in a nanofluid with microorganisms. However, to our best knowledge, no study has been communicated relating to the laminar flow of bioconvective nanofluids past a moveable plate with the blowing effect and multiple slips that include second-order velocity and microorganism slips.

The goal of the present study is to extend a recent work of Uddin et al. [54] by incorporating second order slip and microorganism slip. This study is relevant to the investigation of stretchable walls of microbial nanofluid fuel cells or in bio-nanofluid materials processing systems exploiting bioconvection. Similarity transformations are applied to derive the similarity boundary value problem from the governing equations of the flow model. Effects of selected control parameters (first order slip, second order slip, thermal slip, microorganism slip, blowing, nanofluid parameters) involved in the model on the non-dimensional velocity, temperature, nanoparticle volume fraction and density of motile micro-organism are scrutinized. Verification of our computation is made with previous studies and also with a Nakamura tri-diagonal finite difference method (**NTM**) [55].

2. **MATHEMATICAL MODEL OF NANOFLUID BIOCONVECTION**

We now describe the model of a 2D steady nanofluid-flow containing microorganisms past a moving plate in a clam free stream. The associated coordinate system with the flow model is shown in Fig. 1 in which we choose a Cartesian coordinate system ($\bar{x}$, $\bar{y}$) where $\bar{x}-$ axis is aligned along the plate and $\bar{y}-$ axis, normal to the plate. The plate-velocity can be calculated by

$\bar{u}_w\left(\bar{x}/L\right)=U_r\left(\dfrac{\bar{x}}{L}\right)^{1/5}$, where L denotes the plate length.

Stationary free stream T_∞, C_∞, $\bar{p}_\infty$, n_∞

$\bar{y},\bar{v}$

δ_m δ_T δ_C δ_n

$\bar{x},\bar{u}$

$\bar{v}=-\dfrac{D_B}{1-C_w}\left(\dfrac{\partial C}{\partial \bar{y}}\right),\bar{u}=\bar{u}_w+\bar{u}_{\text{slip}},T=T_w+T_{\text{slip}},C=C_w+C_{\text{slip}},n=n_w+n_{\text{slip}}$
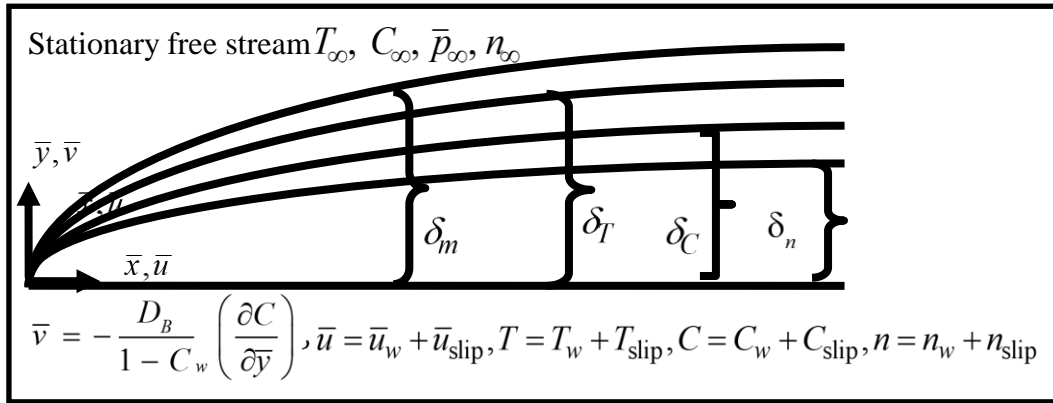
Fig. 1: Coordinate system for nano-bioconvective flow model with multiple slips

The following notations are used for different quantities: T denotes the temperature; C, the nanoparticle volume-fraction; and n, the concentration of motile microorganisms. Subscript ∞ is used to denote the ambient value of the associated quantity while w denotes the value at the

boundary wall. Conservation equations for mass, momentum, energy, nanoparticles and microorganism (Uddin et al. [54]) are expressed by

$$\frac{\partial \bar{u}}{\partial \bar{x}} + \frac{\partial \bar{v}}{\partial \bar{y}} = 0, \tag{1}$$

$$\rho_f \left(\bar{u} \frac{\partial \bar{u}}{\partial \bar{x}} + \bar{v} \frac{\partial \bar{u}}{\partial \bar{y}} \right) = -\frac{\partial \bar{p}}{\partial \bar{x}} + \mu \frac{\partial^2 \bar{u}}{\partial \bar{y}^2}, \tag{2}$$

$$-\frac{\partial \bar{p}}{\partial \bar{y}} + \left[(1 - C_\infty) \rho_f \, g \, \beta (T - T_\infty) - (\rho_{\bar{p}} - \rho_f) g (C - C_\infty) \right] + \gamma (\rho_{\bar{p}} - \rho_f) g (n - n_\infty) = 0, \tag{3}$$

$$\bar{u} \frac{\partial T}{\partial \bar{x}} + \bar{v} \frac{\partial T}{\partial \bar{y}} = \alpha \frac{\partial^2 T}{\partial \bar{y}^2} + \tau \left[D_B \frac{\partial C}{\partial \bar{y}} \frac{\partial T}{\partial \bar{y}} + \left(\frac{D_T}{T_\infty} \right) \left(\frac{\partial T}{\partial \bar{y}} \right)^2 \right], \tag{4}$$

$$\bar{u} \frac{\partial C}{\partial \bar{x}} + \bar{v} \frac{\partial C}{\partial \bar{y}} = D_B \frac{\partial^2 C}{\partial \bar{y}^2} + \left(\frac{D_T}{T_\infty} \right) \frac{\partial^2 T}{\partial \bar{y}^2}, \tag{5}$$

$$\bar{u} \frac{\partial n}{\partial \bar{x}} + \bar{v} \frac{\partial n}{\partial \bar{y}} + \frac{\partial}{\partial \bar{y}} (n \tilde{v}) = D_n \frac{\partial^2 n}{\partial \bar{y}^2}. \tag{6}$$

Boundary conditions [53, 59] are considered as

$$\bar{u} = \bar{u}_w (\bar{x}/L) + \bar{u}_{\text{slip}}, \quad \bar{v} = -\frac{D_B}{1 - C_w} \left(\frac{\partial C}{\partial \bar{y}} \right), \, T = T_w (\bar{x}/L) + T_{\text{slip}} (\bar{x}/L), \, C = C_w (\bar{x}/L) + C_{\text{slip}} (\bar{x}/L)$$

$$n = n_w (\bar{x}/L) + n_{\text{slip}} (\bar{x}/L) \text{ at } \bar{y} = 0, \tag{7}$$

$$\bar{u} \to 0, \, T \to T_\infty, \, C \to C_\infty, \, \bar{p} \to \bar{p}_\infty, n \to 0 \text{ as } \bar{y} \to \infty,$$

where the following notation applies:

Brownian diffusion coefficient	D_B
Thermophoretic diffusion coefficient	D_T
Diffusivity of microorganisms	D_n
gravitational acceleration	g
effective thermal conductivity	k
Velocity components along the $\bar{x}$ and $\bar{y}$	$(\bar{u}, \bar{v})$
thermal diffusivity of the fluid	α
volumetric expansion coefficient of nanofluid	β
density of the base fluid	ρ_f
density of the nanoparticles	$\rho_{\bar{p}}$
dynamic viscosity of the base fluid	μ
effective heat capacity of the fluid	$(\rho c)_f$
effective heat capacity of the nanoparticles	$(\rho c)_{\bar{p}}$

Characteristic velocity	$U_r = \dfrac{\alpha}{L} Ra^{2/5}$
Swimming velocity of microorganism along y direction	$\tilde{v} = \dfrac{\tilde{b} W_c}{\Delta C} \dfrac{\partial C}{\partial \bar{y}}$
Ratio of effective heat capacity of the nanoparticle to effective heat capacity of the fluid	$\tau = \dfrac{(\rho c)_{\bar{p}}}{(\rho c)_f}$

Furthermore, velocity slip is given by:

$$\bar{u}_{\text{slip}} = \frac{2}{3}\left(\frac{3 - \bar{\alpha}\, l^3}{\bar{\alpha}} - \frac{2}{3}\frac{1 - l^2}{K_n} \right) \lambda\left(\bar{x}/L\right)\frac{\partial \bar{u}}{\partial \bar{y}} - \frac{1}{4}\left[l^4 + \frac{2}{K_n^2}\left(1 - l^2\right) \right]\lambda^2\left(\bar{x}/L\right)\frac{\partial^2 \bar{u}}{\partial \bar{y}^2}, l = \min\left[\frac{1}{K_n}, 1 \right], \qquad (8)$$

$$= N_1\left(\bar{x}/L\right)\frac{\partial \bar{u}}{\partial \bar{y}} + N_2\left(\bar{x}/L\right)\frac{\partial^2 \bar{u}}{\partial \bar{y}^2},$$

where the following notation applies:

Momentum accommodation coefficient	$0 \le \bar{\alpha} \le 1$
Molecular mean free path	λ
Knudsen number	K_n
First order slip factor	$N_1\left(\bar{x}/L\right) = \dfrac{2}{3}\left(\dfrac{3 - \bar{\alpha}\, l^3}{\bar{\alpha}} - \dfrac{2}{3}\dfrac{1 - l^2}{K_n} \right)\lambda\left(\bar{x}/L\right)$
Second order slip factor	$N_2\left(\bar{x}/L\right) = -\dfrac{1}{4}\left[l^4 + \dfrac{2}{K_n^2}\left(1 - l^2\right) \right]\lambda^2\left(\bar{x}/L\right)$
Thermal slip	$T_{\text{slip}}(x) = D_1(x)\dfrac{\partial T}{\partial \bar{y}}$
Mass (nanoparticle species) slip	$C_{\text{slip}}(x) = E_1(x)\dfrac{\partial C}{\partial \bar{y}}$
Micro-organism slip	$n_{\text{slip}}(x) = F_1(x)\dfrac{\partial n}{\partial \bar{y}}$

The multiple slip factors are assumed to take the form:

$$N_1(x) = \left(N_1\right)_0 (x)^{2/5}$$
$$N_2(x) = \left(N_2\right)_0 (x)^{3/5}$$
$$D_1(x) = \left(D_1\right)_0 (x)^{2/5}$$
$$E_1(x) = \left(E_1\right)_0 (x)^{2/5}$$
$$F_1(x) = \left(F_1\right)_0 (x)^{2/5},$$

where:

Constant First-order velocity slip factor	$\left(N_1\right)_0$

Constant Second order velocity slip factor $(N_2)_0$

Constant thermal slip factor $(D_1)_0$

Constant mass slip factor $(E_1)_0$

Constant micro-organism slip factor $(F_1)_0$

Gas flow in micro channels can be classified into four categories [**60**] considering the variation of Knudsen number (K_n), (i) continuum flow regime ($K_n \leq 0.001$); (ii) slip flow regime ($0.001 \leq K_n \leq 0.1$); (iii) transition flow regime ($0.1 \leq K_n \leq 10$) and (iv) free molecular flow regime ($K_n \geq 10$).

In order to transform Eqns. (1)-(7) into non-dimensional form [61], the following variables are introduced:

$$x = \frac{\bar{x}}{L}, \ y = \frac{\bar{y}}{L} Ra^{1/5}, \ u = \frac{L}{\alpha} Ra^{-2/5}\bar{u}, \ v = \frac{L}{\alpha} Ra^{-1/5}\bar{v}, \ \theta = \frac{T - T_\infty}{T_w - T_\infty},$$

$$\phi = \frac{C - C_\infty}{C_w - C_\infty}, \ \chi = \frac{n}{n_w}, \ p = \frac{L^2(\bar{p} - \bar{p}_\infty)}{\rho_f \alpha^2} Ra^{-4/5}, \tag{9}$$

in which $Ra = g\beta(1 - C_\infty)(T_w - T_\infty)L^3\rho_f / (\alpha\mu)$ is the Rayleigh number. Moreover, using Cauchy-Riemann equations, we use a stream function ψ defined by $u = \frac{\partial \psi}{\partial y}$; $v = -\frac{\partial \psi}{\partial x}$, which identically satisfies Eqn. (1). We now employ a group of similarity transformations [55]:

$$\eta = \frac{y}{x^{\frac{2}{5}}}, \ \psi = x^{\frac{3}{5}}f(\eta), \ p = x^{\frac{2}{5}}h(\eta), \ \theta = \theta(\eta), \ \phi = \phi(\eta), \ \chi = \chi(\eta), \tag{10}$$

in Eqns. (2)-(6) we get the following equations

$$\Pr f''' + \frac{3}{5} f f'' - \frac{1}{5} f'^2 + \frac{2}{5}\eta \ h' - \frac{2}{5} h = 0, \tag{11}$$

$$-\frac{1}{\Pr} h' + \theta - Nr \ \phi + Rb \ \chi = 0, \tag{12}$$

$$\theta'' + \frac{3}{5} f \ \theta' + Nb \ \theta' \ \phi' + Nt \ \theta'^2 = 0, \tag{13}$$

$$\phi'' + \frac{3}{5} Le f \ \phi' + \frac{Nt}{Nb}\theta'' = 0, \tag{14}$$

$$\chi'' - Pe(\phi' \chi' + \chi \phi'') + \frac{3}{5} Lb f \ \chi' = 0. \tag{15}$$

The boundary conditions are re-formulated as:

$$f(0) = \frac{5s}{3Le}\phi'(0), \ f'(0) = 1 + a\ f''(0) + b\ f'''(0), \ \theta(0) = 1 + c\ \theta'(0), \ \phi(0) = 1 + d\ \phi'(0),$$

$$\chi(0) = 1 + e\chi'(0), \ f'(\infty) = \theta(\infty) = \phi(\infty) = h(\infty) = \chi(\infty) = 0,$$

(16)

where the terms are defined as

Dimensionless velocity	$f(\eta)$
Dimensionless temperature	$\theta(\eta)$
Dimensionless nanoparticle volume-fraction (concentration)	$\phi(\eta)$
Dimensionless microorganism concentration	$\chi(\eta)$
Prandtl number	$\Pr = \dfrac{\nu}{\alpha}$
Thermophoresis	$Nt = \dfrac{\tau D_T (T_w - T_\infty)}{\alpha T_\infty}$
Brownian motion	$Nb = \dfrac{\tau D_B (C_w - C_\infty)}{\alpha}$
Buoyancy ratio	$Nr = \dfrac{(\rho_p - \rho_f)(C_w - C_\infty)}{\rho_f \beta (1 - C_\infty)(T_w - T_\infty)}$
Lewis number	$Le = \dfrac{\alpha}{D_B}$
First order velocity slip	$a = \dfrac{(N_1)_0 \mu Ra^{2/5}}{\rho_f L}$
Second order velocity slip	$b = \dfrac{(N_2)_0 \mu Ra^{2/5}}{\rho_f L}$
Thermal slip	$c = \dfrac{(D_1)_0 Ra^{2/5}}{L}$
Mass slip	$d = \dfrac{(E_1)_0 Ra^{2/5}}{L}$
Microorganism slip	$, e = \dfrac{(F_1)_0 Ra^{2/5}}{L}$
Bioconvection Rayleigh number	$Lb = \nu / D_n$
Bioconvection Péclet number	$Pe = \dfrac{\tilde{b}W_c}{D_n}$
Bioconvection Lewis number	$Rb = \gamma(\rho_p - \rho_{f\infty})(n_w - n_\infty)/(T_w - T_\infty)\beta(1 - C_\infty)$
Stefan blowing	$s = \dfrac{D_B (C_w - C_\infty)}{\alpha(1 - C_w) Ra^{-3/5}}.$

4. PHYSICAL QUANTITIES

Certain physical quantities i.e., local skin friction factor $C_{f\bar{x}}$, local Nusselt number $Nu_{\bar{x}}$, local Sherwood number $Sh_{\bar{x}}$, local density number of the motile microorganisms $Nn_{\bar{x}}$, are important for engineering applications e.g., in the proximity of near-wall flows of microbial nano-bioconvection fuel cell design and in nano-bio-materials processing systems. The quantities are computed by the following expressions:

$$C_{f\bar{x}} = \frac{2\mu}{\rho\bar{u}_w^2}\left(\frac{\partial\bar{u}}{\partial\bar{y}}\right)_{\bar{y}=0}, \quad Nu_{\bar{x}} = \frac{-\bar{x}}{T_w-T_\infty}\left(\frac{\partial T}{\partial\bar{y}}\right)_{\bar{y}=0}, Sh_{\bar{x}} = \frac{-\bar{x}}{C_w-C_\infty}\left(\frac{\partial C}{\partial\bar{y}}\right)_{\bar{y}=0}, \quad Nn_{\bar{x}} = \frac{-\bar{x}}{n_w-n_\infty}\left(\frac{\partial n}{\partial\bar{y}}\right)_{\bar{y}=0}.$$

(17)

Using the transformations, Eqn. (16) in Eqn. (23), one derives that

$$Ra_{\bar{x}}^{3/5} C_{f\bar{x}} = f''(0), \ Ra_{\bar{x}}^{-1/5} Nu_{\bar{x}} = -\theta'(0), Ra_{\bar{x}}^{-1/5} Sh_{\bar{x}} = -\phi'(0), Ra_{\bar{x}}^{-1/5} Nn_{\bar{x}} = -\chi'(0).$$

(18)

where $Ra_{\bar{x}} = g\beta(1-C_\infty)\Delta T \bar{x}^3/(\alpha\nu)$ is the local Rayleigh number.

5. COMPUTATIONAL SOLUTION OF NANOFLUID-BIOCONVECTION MODEL

Transformation of the original flow model into ordinary differential equations (ODEs) (11)–(15) with boundary conditions (16) significantly reduces the computation. The objective is now to solve the ODEs efficiently. Since the equations contain higher order terms, they need to be formulated as a set of first order ODEs. Assume that $z_1 = f$, $z_2 = \theta, z_3 = \phi, z_4 = \chi, z_5 = h, z_6 = f'$ $z_7 = \theta'$, $z_8 = \phi', z_9 = \chi'$, $z_{10} = f'' = z_6'$. With these variables in Eqns. (11)–(15), the following system of ODEs is reconstructed:

$$\underbrace{\begin{bmatrix} z_1' \\ z_2' \\ z_3' \\ z_4' \\ z_5' \\ z_6' \\ z_7' \\ z_8' \\ z_9' \\ z_{10}' \end{bmatrix}}_{z'} = \underbrace{\begin{bmatrix} z_6 \\ z_7 \\ z_8 \\ z_9 \\ z_2 - Nr\, z_3 + Rbz_4 \\ z_{10} \\ -z_7\left[\frac{3}{5}z_1 + Nb\, z_8 + Nt\, z_7\right] \\ -\frac{3}{5}Le\, z_1 z_8 + \frac{Nt}{Nb}z_7\left[\frac{3}{5}z_1 + Nb\, z_8 + Nt\, z_7\right] \\ z_9\left(Pe\, z_8 - \frac{3}{5}Lb\, z_1\right) + Pe\, z_4\left(-\frac{3}{5}Le\, z_1 z_8 + \frac{Nt}{Nb}z_7\left[\frac{3}{5}z_1 + Nb\, z_8 + Nt\, z_7\right]\right) \\ \frac{1}{Pr}\left(\frac{z_6^2}{5} - \frac{3}{5}z_1 z_{10} + \frac{2}{5}z_5 - \frac{2}{5}\eta[z_2 - Nr\, z_3 + Rbz_4]\right) \end{bmatrix}}_{g(z)}$$

(19)

In this system of equations, we have a vector $z = [z_1, z_2, z_3, z_4, z_5, z_6, z_7, z_8, z_9, z_{10}]^T$ of ten variables with ten equations in Eqn. (19). We highlight that the velocity slip boundary condition in Eqn. (16) includes a third derivative term which has to be converted to a condition comprising lower order derivatives. We convert the velocity slip boundary condition using Eqn. (16) with Eqn. (11) as follows:

$$f'(0) = 1 + af''(0) + bf'''(0)$$
$$= 1 + af''(0) + \frac{b}{Pr} - 0.6f(0)f''(0) + 0.2f'^2(0) + 0.4h(0)$$

From the above equation, we deduce that:

12

$$f''(0) = \frac{f'(0) - 1 - \frac{b}{Pr}\left[0.2 f'^2(0) + 0.4h(0)\right]}{a - \frac{0.6b}{Pr} f(0)}$$

Finally, the boundary conditions Eqn. (16) can be expressed as:

$$
\left.
\begin{array}{l}
z_1(0) = \frac{5s}{3Le}\, z_8(0) \\[4pt]
z_2(0) = 1 + cz_7(0) \\[2pt]
z_3(0) = 1 + dz_8(0) \\[2pt]
z_4(0) = 1 + ez_9(0) \\[2pt]
z_5(0) = \text{unknown} \\[2pt]
z_6(0) = \text{unknown} \\[2pt]
z_7(0) = \text{unknown} \\[2pt]
z_8(0) = \text{unknown} \\[2pt]
z_9(0) = \text{unknown} \\[2pt]
z_{10}(0) = \frac{z_6(0) - 1 - b[0.2\, z_6^2 + 0.4z_5(0)]/Pr}{a - 0.6z_1/Pr}
\end{array}
\right\}
\tag{20}
$$

Observe that the initial conditions $z_5(0) - z_9(0)$ are unknown that inhibits solving Eqn. (19) directly. However, one can use following additional boundary conditions

$$
\left.
\begin{array}{l}
z_2(\infty) = 0 \\[2pt]
z_3(\infty) = 0 \\[2pt]
z_4(\infty) = 0 \\[2pt]
z_5(\infty) = 0 \\[2pt]
z_6(\infty) = 0
\end{array}
\right\}
\tag{21}
$$

to solve the system. Eqn. (21) takes the form of a *nonlinear* system of equations in which we attempt to find the unknowns in Eqn. (20) such that (21) holds. It is noticed that $\eta = 20$ is adequate to represent a sufficiently large $\eta \to \infty$. The following algorithm constructs Eqn. (21) as a system of nonlinear equations.

Algorithm 1: Construction of Function $F(q)$

Input: $q \in \mathbb{R}^5$

Output : $t \in \mathbb{R}^5$

1. Assign the unknown values as

$$
\begin{bmatrix} z_5(0) \\ z_6(0) \\ z_7(0) \\ z_8(0) \\ z_9(0) \end{bmatrix}
:=
\begin{bmatrix} q_1 \\ q_2 \\ q_3 \\ q_4 \\ q_5 \end{bmatrix}
$$

2. Compute $[z_1(20), z_2(20), \ldots, z_{10}(20)]$ by solving (19) with (20) taking the unknown values in step 1 using Matlab function *ode15s*.

3. Assign the output t as

$$
\begin{bmatrix} t_1 \\ t_2 \\ t_3 \\ t_4 \\ t_5 \end{bmatrix}
:=
\begin{bmatrix} z_2(20) \\ z_3(20) \\ z_4(20) \\ z_5(20) \\ z_6(20) \end{bmatrix}
$$

4. Return t

13

In Algorithm 1, the function $F(q)$ is formulated that can be computed for a given input values of $q:=[q_1, q_2, q_3, q_4, q_5]^T$. Values of q are set to the unknowns of (20). Eqn. (19) can then be solved by Matlab stiff ODE solver *ode15s* that produces the solution as $[z_1(20), z_2(20), ..., z_{10}(20)]^T$. We select the values releated to additional boundary conditions and them to $[t_1, t_2, t_3, t_4, t_5]^T$ which is the output from the function. Now our goal is to find a solution q such that the following condition holds:

$$F(q) = 0 \tag{21}$$

which has the form of a highly nonlinear system of equations. Eqn. (21) can be solved by Matlab trust-region-reflective algorithm *fsolve*.

6. VALIDATION OF MATLAB COMPUTATION

Comparison of a simplified version of our model with existing solutions in the literature was made to verify our solution of the model. In the absence of blowing ($s = 0$), slip boundary conditions ($a = c = d = e = 0$) and microorganism equation (Eqn. (16)), our model takes the form of the model from Pradhan *et al.* [58] for a stationary sheet ($f'(0) = 0$). For this case, we compared our test results with those of Pradhan *et al.* in Table 1 where an excellent agreement is achieved in the comparison. The reason for not having an exact match (slight variation) is that our computation has an accuracy of the order $O(10^{-10})$, while Pradhan *et al* [58] used an accuracy of $O(10^{-8})$ for their solution.

To examine the nano-bioconvective flow with multiple slips, we carried out computational tests with different values of thermophysical parameters. In our tests, a water based nanofluid is considered with the parameters as follows: $Pr = 6.8$ (water), $Nb = Nr = Nt = 0.1$, $Pe = Lb = Rb = 1$, $Le = 10$ unless stated otherwise. **Tables 2-3** present the solutions which have been benchmarked with an alternative numerical method of Nakamura [55] which easily solves the coupled boundary value problems. Similar to Keller-Box approach, in Nakamura tri-diagonal method (**NTM),** the higher order differential equations are reduced in order. The method has been used for solving many boundary layer problems e.g., viscoelastic polymer flows, non- magnetohydrodynamics, Newtonian heat transfer and transient rotating flows [62-65]. Solution procedure using **NTM** for our nano-bioconvective flow model can be presented as follows.

Our goal is to solve eqns. (11)-(16) which are third-order ODEs which are required to be transformed to second-order ODEs. The following substitutions are used.

$$J = f', \ K = h, \ L = \theta, M = \phi, \ N = \zeta \tag{29}$$

The eqns. (17)-(21) take the form:

Nakamura momentum equation:

$$A_1 J'' + B_1 J' + C_1 J = S_1 \tag{30}$$

Nakamura pressure equation:

$$A_2 K'' + B_2 K' + C_2 K = S_2 \tag{31}$$

Nakamura energy (heat) equation:

$$A_3L^{//} + B_3L^{/} + C_3L = S_3 \tag{32}$$

Nakamura species (nanoparticle concentration) equation:

$$A_4M^{//} + B_4M^{/} + C_4M = S_4 \tag{33}$$

Nakamura motile microorganism density equation:

$$A_5L^{//} + B_5L^{/} + C_5L = S_5 \tag{34}$$

where $A_{i=1...5}$, $B_{i=1..5}$, $C_{i=1..5}$ are the *Nakamura matrix coefficients*, $S_{i=1...5}$ are the *Nakamura source terms*. The source term includes the variables and derivatives which do not depend on lead variables. For instance, in eqn. (31), the source term does not include any term comprising the lead variable *K*. To proceed with **NTM**, an equi-spaced finite difference mesh is used to discretize the one-dimensional domain in η-direction. Differentiations of *f, h, θ, ϕ* and χ with respect to η are computed by the central difference scheme. Thus eqns. (30)-(34) are converted to finite difference equations which are then formulated as a tri-diagonal system. The 10 boundary conditions in eqn. (16) are set in the system by modifying the rows/columns at appropriate positions. An iteration loop is used to compute the solutions of the momentum, pressure, energy, nanoparticle species (concentration) and motile microorganism density conservation equations by successive substitution at each iteration due to the high nonlinearity of equations. Specifically, at each iteration, solutions are obtained by solving tri-diagonal system modified by the boundary conditions. **NTM** solutions were compared with the results of Pradhan *et al.* [**58**] where a good agreement is achieved in comparison. Furthermore, general model solutions obtained with **MATLAB** are compared with **NTM** computations that provided a good correlation. Hence, the accuracy in the **MATLAB** code is high.

Table 1: Comparison of present study with Pradhan *et al.* [58] on skin friction factor $f''(0)$ and heat transfer rate $-\theta'(0)$ with $s=a = c =$d=e = 0, $f'(0) = 0$, *Le* = 10 and *Pr* = 7.

Nb	*Nt*	*Nr*	$f''(0)$			$-\theta'(0)$		
			Present Study	Pradhan *et al.* [58]	NTM	Present Study	Pradhan *et al.* [58]	NTM
0.1	0.2	0.4	0.859828	0.86002	0.86114	0.357423	0.35744	0.35739
0.5			0.929720	0.92979	0.92981	0.268031	0.26799	0.26795
0.3	0.1	0.001	0.953720	0.95374	0.95371	0.328791	0.32878	0.32873
		0.1	0.939522	0.93956	0.93958	0.327855	0.32784	0.32781
		0.2	0.925020	0.92507	0.92509	0.326894	0.32688	0.32684
		0.3	0.910352	0.91042	0.91044	0.325917	0.32591	0.32588
		0.5	0.880486	0.88058	0.88057	0.323914	0.32391	0.32387
	0.001	0.2	0.913447	0.91340	0.91341	0.340780	0.34076	0.34072
	0.2		0.936959	0.93704	0.93705	0.313637	0.31362	0.31359
	0.5		0.973797	0.97398	0.97396	0.277959	0.27797	0.27795

Table 2: Skin friction factor $f''(0)$ and wall mass flux of motile microorganism $-\chi'(0)$ with various values of *a, b, c, d, e* and *s*.

s	a	b	c	d	e	$f''(0)$	$f''(0)$	$-\chi'(0)$	$-\chi'(0)$

s	a	b	c	d	e	MATLAB	NTM	MATLAB	NTM
-1						0.2345347	0.234535	2.464943	2.464945
0	0.1	-0.1	0.1	0.1	0.1	0.3554415	0.355442	1.700089	1.700090
1						0.4154311	0.414532	1.323610	1.323612
-1	10	-0.1				0.0335244	0.033528	2.589387	2.589388
0	10	-0.1	0.1	0.1	0.1	0.0505944	0.050595	1.884324	1.884326
1	10	-0.1				0.0594578	0.059458	1.507185	1.507187
-1	0.1	0				-0.1852024	-0.185303	2.445849	2.445855
0	0.1	0	0.1	0.1	0.1	-0.1473831	-0.147385	1.678216	1.678220
1	0.1	0				-0.1300381	-0.130038	1.304167	1.304170
-1	0.1	-5				-0.4264349	-0.426437	2.814376	2.814376
0	0.1	-5	0.1	0.1	0.1	-0.431085	-0.431082	2.125818	2.125821
1	0.1	-5				-0.4346665	-0.436671	1.722904	1.722905
-1	0.1	-0.1				0.2559226	0.255923	2.457017	2.457019
0	0.1	-0.1	0	0.1	0.1	0.3742363	0.374236	1.701444	1.701446
1	0.1	-0.1				0.433374	0.433376	1.326461	1.326465
-1	0.1	-0.1				-0.0044658	-0.004467	2.558446	2.558447
0	0.1	-0.1	5	0.1	0.1	0.1031409	0.103141	1.679545	1.679549
1	0.1	-0.1				0.1569777	0.156978	1.281188	1.281192
-1	0.1	-0.1				-0.0128258	-0.012826	4.813505	4.813508
0	0.1	-0.1	0.1	0	0.1	0.3357962	0.335796	1.903316	1.903319
1	0.1	-0.1				0.4072657	0.407266	1.382789	1.382790
-1	0.1	-0.1				0.3566764	0.356677	1.442593	1.442595
0	0.1	-0.1	0.1	0.5	0.1	0.402758	0.402759	1.281593	1.281597
1	0.1	-0.1				0.4398622	0.439862	1.139594	1.139596
-1	0.1	-0.1				0.2713895	0.271390	3.284665	3.284668
0	0.1	-0.1	0.1	0.1	0	0.3833455	0.382246	2.057325	2.057327
1	0.1	-0.1				0.4385199	0.483520	1.531610	1.531614
-1	0.1	-0.1				0.1254961	0.125496	0.188340	0.188343
0	0.1	-0.1	0.1	0.1	5	0.2270652	0.227066	0.181867	0.181869
1	0.1	-0.1				0.2773583	0.277358	0.176307	0.176310

Table 3: Heat transfer rate $-\theta'(0)$ and wall mass flux of nanoparicles $-\phi'(0)$ with various values of *a, b, c, d, e* and *s*.

s	a	b	c	d	e	$-\theta'(0)$ MATLAB	$-\theta'(0)$ NTM	$-\phi'(0)$ MATLAB	$-\phi'(0)$ NTM
-1						0.690358	0.690356	2.662430	2.662426
0	0.1	-0.1	0.1	0.1	0.1	0.561010	0.561006	1.639821	1.639811
1						0.508482	0.508478	1.195537	1.195533
-1	10	-0.1				0.747340	0.747332	2.826062	2.826061
0	10	-0.1	0.1	0.1	0.1	0.630261	0.630259	1.853659	1.853654
1	10	-0.1				0.578220	0.578214	1.389526	1.389521
-1	0.1	0				0.682081	0.682078	2.637294	2.637289

0	0.1	0	0.1	0.1	0.1	0.553462	0.553460	1.614720	1.614715
1	0.1	0				0.501630	0.501628	1.175148	1.175143
-1	0.1	-5				0.866670	0.866667	3.127368	3.127366
0	0.1	-5	0.1	0.1	0.1	0.733650	0.733649	2.135950	2.135947
1	0.1	-5				0.670867	0.670863	1.621613	1.621610
-1	0.1	-0.1				0.741141	0.741139	2.647089	2.647094
0	0.1	-0.1	0	0.1	0.1	0.595408	0.595405	1.639527	1.639524
1	0.1	-0.1				0.536786	0.536784	1.197341	1.197336
-1	0.1	-0.1				0.157576	0.157574	2.844404	2.844401
0	0.1	-0.1	5	0.1	0.1	0.148409	0.148406	1.642161	1.642165
1	0.1	-0.1				0.144097	0.144094	1.168748	1.168745
-1	0.1	-0.1				0.964090	0.964087	8.277239	8.277236
0	0.1	-0.1	0.1	0	0.1	0.551604	0.551600	1.980785	1.980783
1	0.1	-0.1				0.497632	0.497629	1.309836	1.309835
-1	0.1	-0.1				0.635701	0.635697	1.098599	1.098596
0	0.1	-0.1	0.1	0.5	0.1	0.580834	0.580831	0.968709	0.968708
1	0.1	-0.1				0.540187	0.540183	0.851247	0.851243
-1	0.1	-0.1				0.695301	0.695297	2.671523	2.671519
0	0.1	-0.1	0.1	0.1	0	0.564425	0.564421	1.646283	1.646280
1	0.1	-0.1				0.511061	0.511059	1.199816	1.199813
-1	0.1	-0.1				0.675048	0.675044	2.634885	2.634882
0	0.1	-0.1	0.1	0.1	5	0.544776	0.544772	1.609402	1.609398
1	0.1	-0.1				0.492475	0.492470	1.169337	1.169335

7. COMPUTATIONAL RESULTS AND DISCUSSION

Figs. 2-13 illustrate our numerical results. In all these plots it is evident that $f'(\eta) \to 0$, $\theta(\eta) \to 0$, $\phi(\eta) \to 0$ and $\chi(\eta) \to 0$ *asymptotically* as $\eta \to \infty$. For the current bioconvection nanofluid problem we found that $\eta \to 20$ is large enough to fulfill the boundary condition $\eta \to \infty$. The accuracy of the solutions for $f'(\eta)$, $\phi(\eta)$, $\theta(\eta)$ and $\chi(\eta)$ at $\eta = 20$ is of the order $O(10^{-10})$.
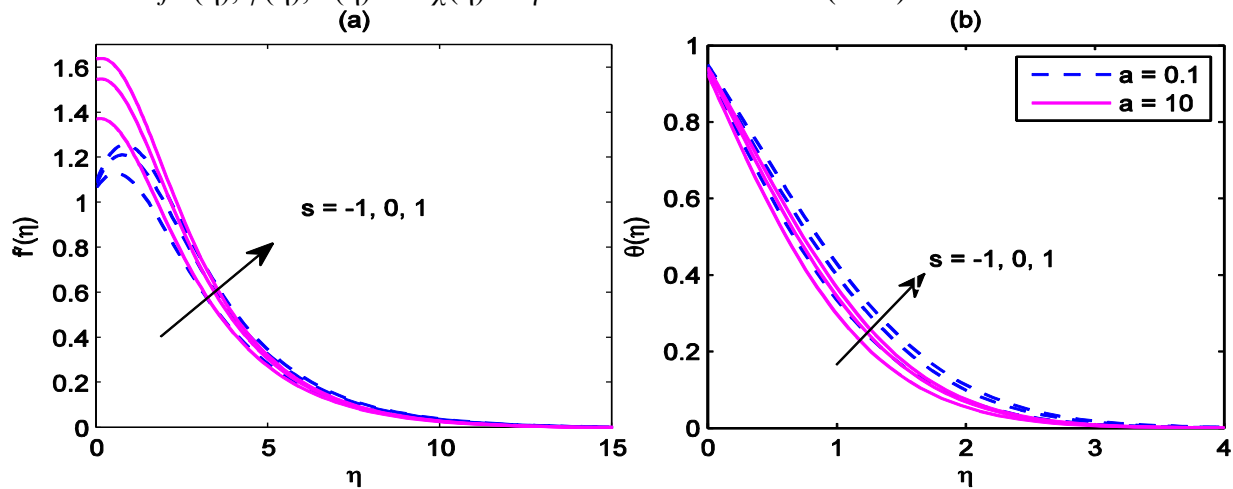

Fig. 2: Variation in profiles of the dimensionless (a) velocity $f'(\eta)$ and (b) temperature $\theta(\eta)$ for different values of velocity slip a and blowing parameter s
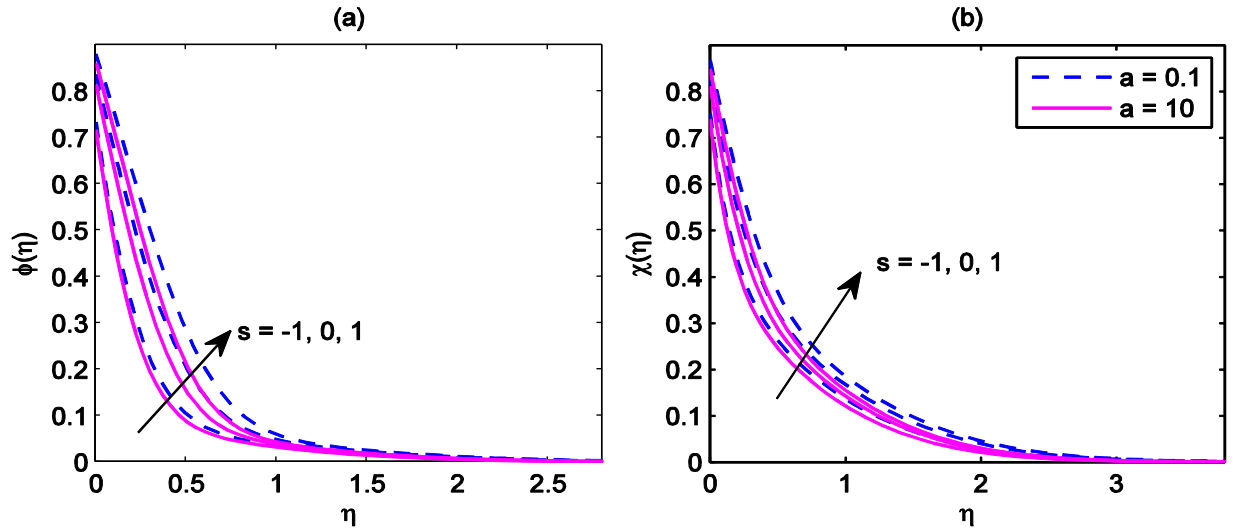
17

Fig. 3: Variation in profiles of the dimensionless (a) nanoparticle volume-fraction $\phi(\eta)$ and (b) microorganism concentration $\chi(\eta)$ for different values of $a = c =$ Nb=0.1, $\lambda = Lb = Pe = 1$, $Le = 10$ for different values of velocity slip parameter a and blowing parameter s
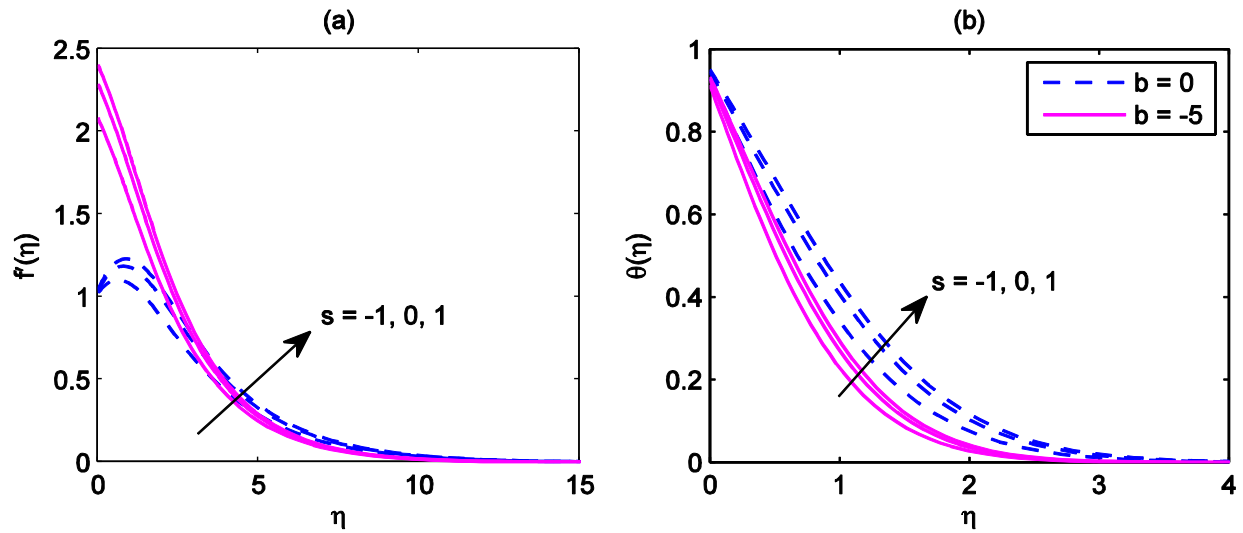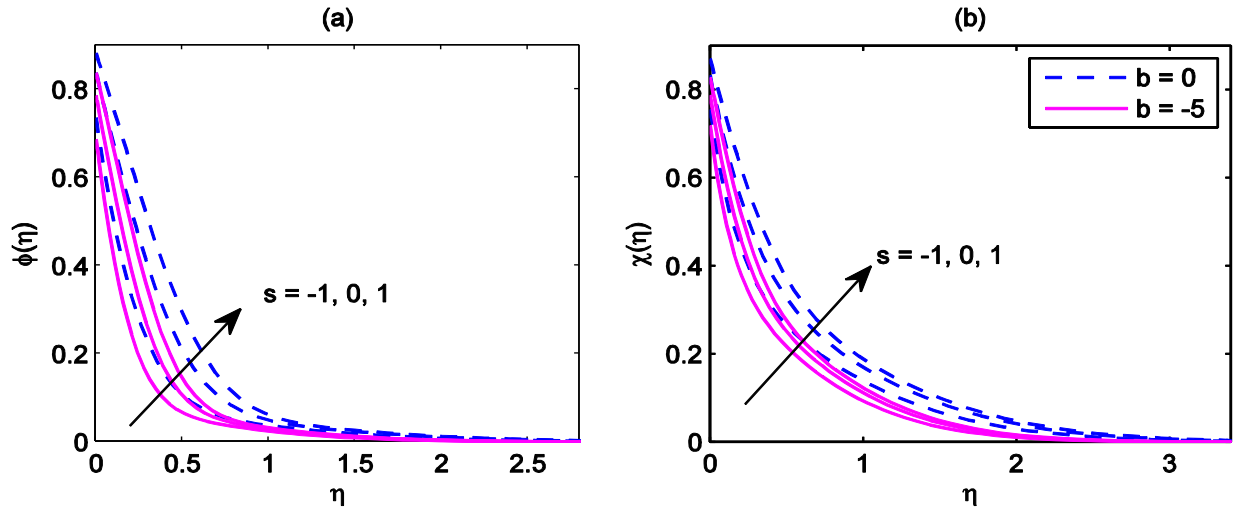

Fig. 4: Variation in profiles of the dimensionless (a) velocity $f'(\eta)$ and (b) temperature $\theta(\eta)$ for second order velocity slip parameter b and blowing parameter s.

Fig. 5: Variation in profiles of the dimensionless (a) nanoparticle volume-fraction $\phi(\eta)$ and (b) microorganism concentration $\chi(\eta)$ for second order velocity slip parameter b and blowing parameter s.
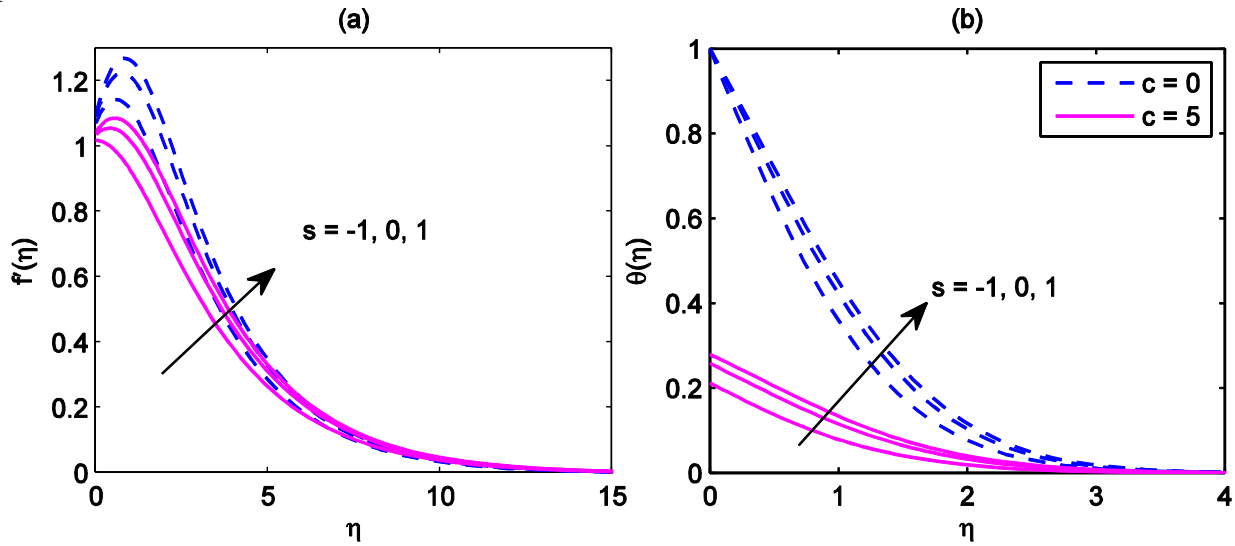
Fig. 6: Variation in profiles of dimensionless (a) velocity $f'(\eta)$ and (b) temperature $\theta(\eta)$ for thermal slip parameter c and blowing parameter s.
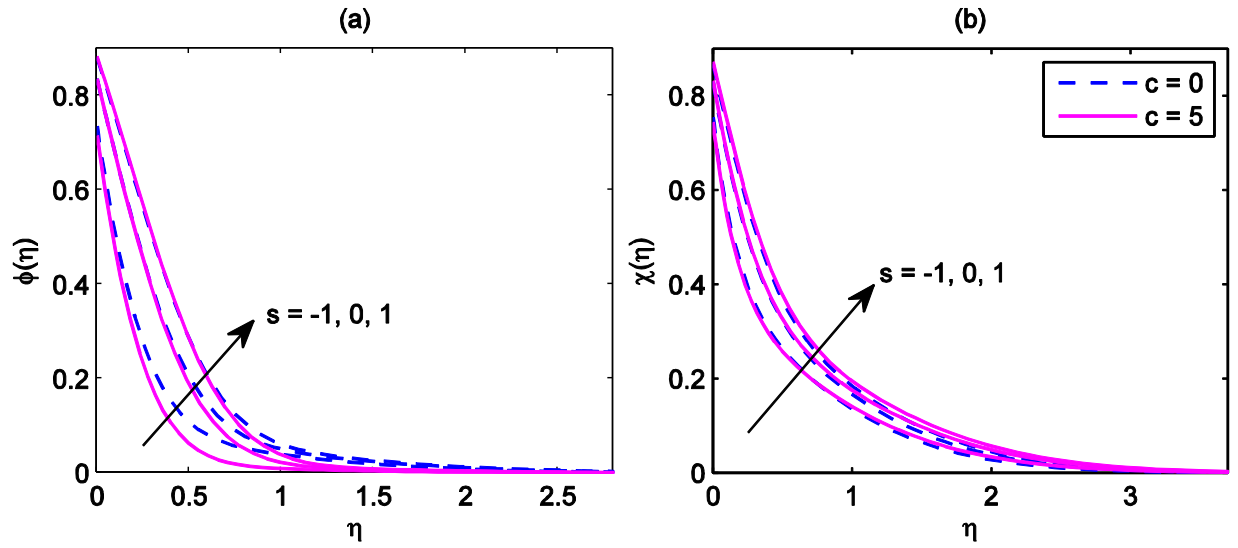
Fig. 7: Variation of dimensionless (a) nanoparticle volume-fraction $\phi(\eta)$ and (b) microorganism concentration $\chi(\eta)$ for thermal slip parameter c and blowing parameter s.
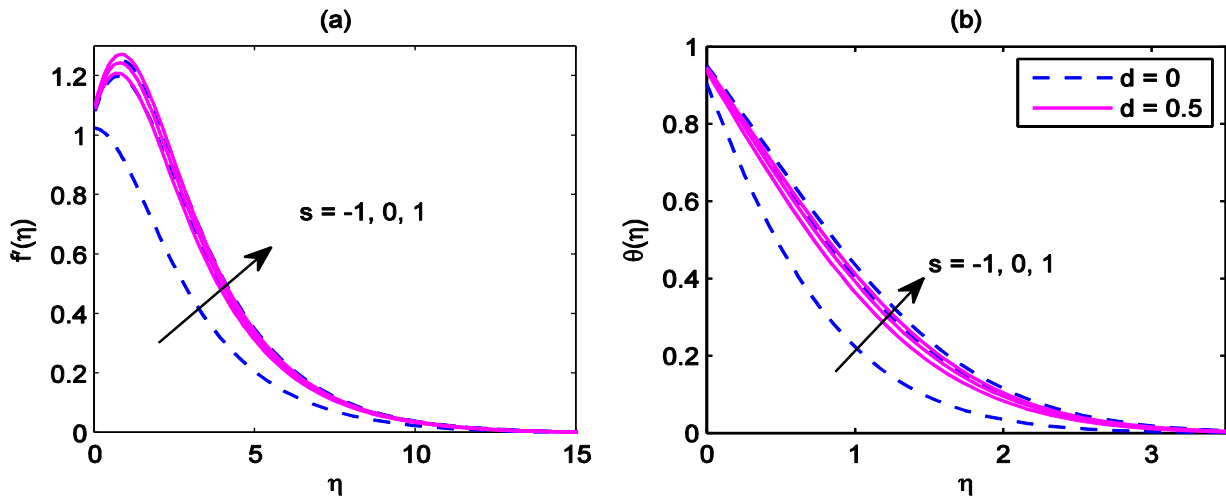

Fig. 8: Variation of dimensionless (a) velocity $f'(\eta)$ and (b) temperature $\theta(\eta)$ for solutal slip parameter d and blowing parameter s.
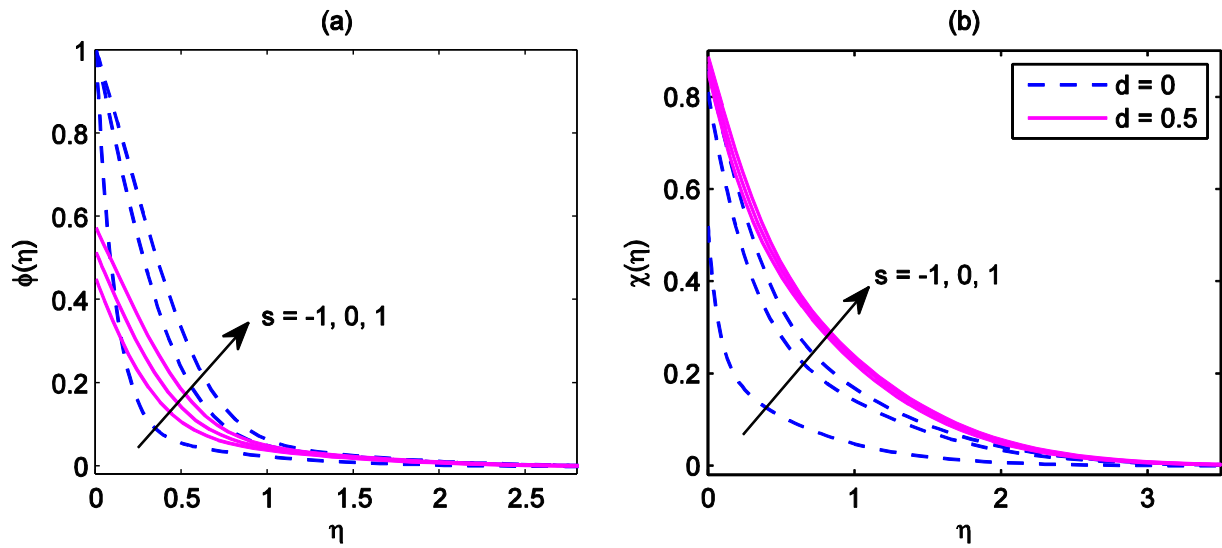
Fig. 9: Variation of dimensionless (a) nanoparticle volume fraction $\phi(\eta)$ and (b) microorganism concentration $\chi(\eta)$ for solutal slip parameter d and blowing parameter s.
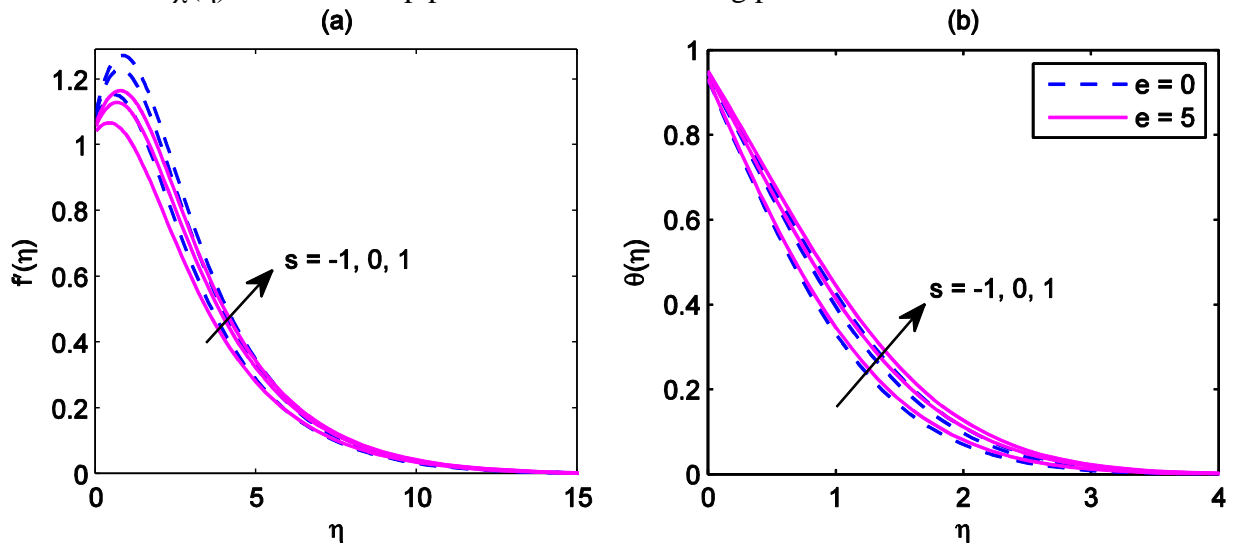

Fig. 10: Variation of dimensionless (a) velocity $f'(\eta)$ and (b) temperature $\theta(\eta)$ for microorganism slip parameter e and blowing parameter s.
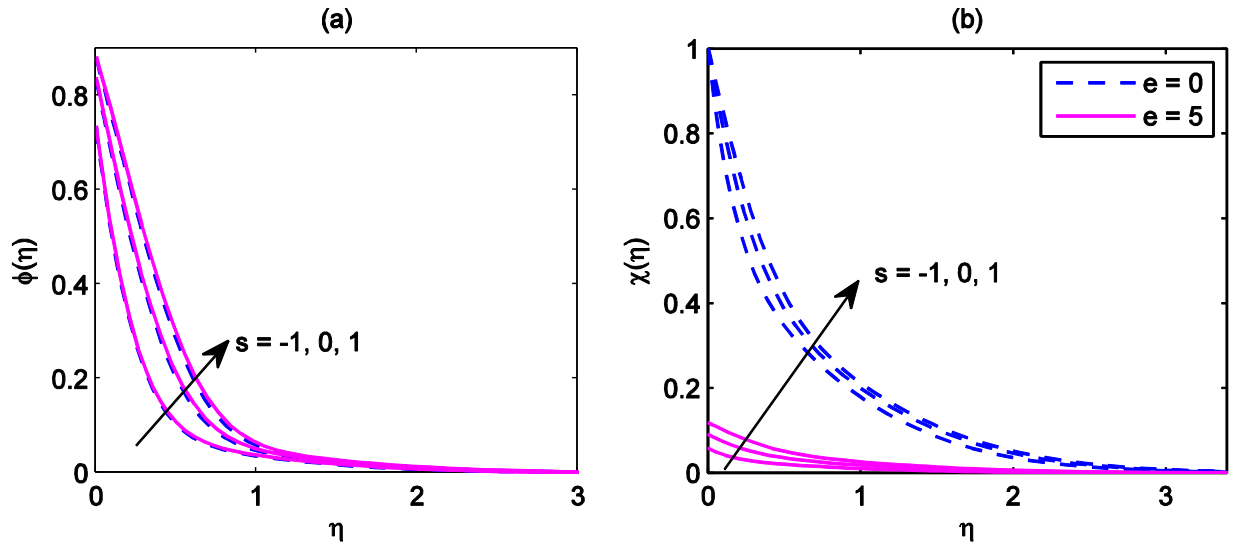
21

Fig. 11: Variation of dimensionless (a) nanoparticle volume fraction $\phi(\eta)$ and (b) microorganism concentration $\chi(\eta)$ for the microorganism slip parameter e and blowing parameter s.
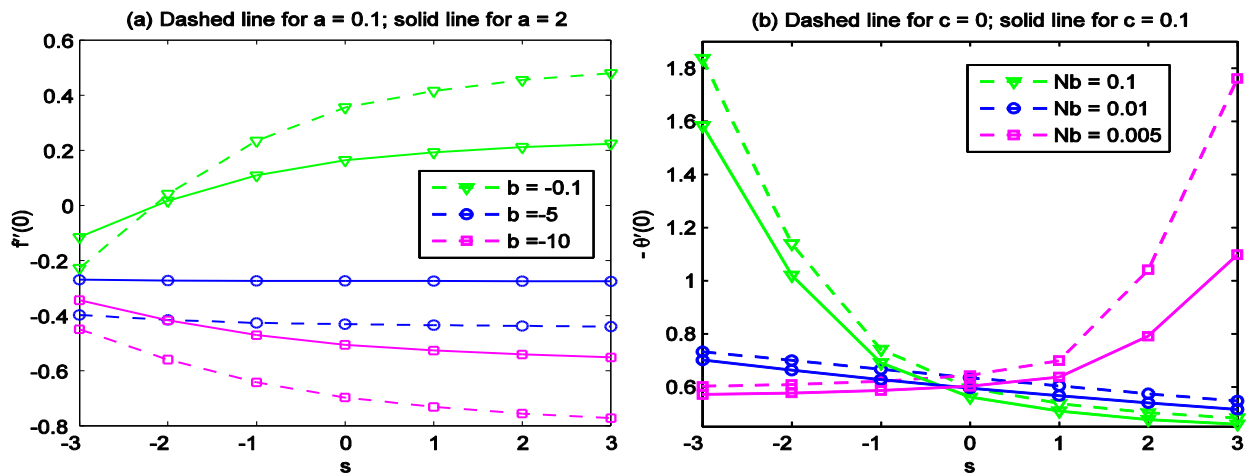

Fig. 12: (a) Effect of velocity slips a and b on skin friction factor $f''(0)$ and (b) effect of c and Nb on heat transfer rate $-\theta'(0)$.
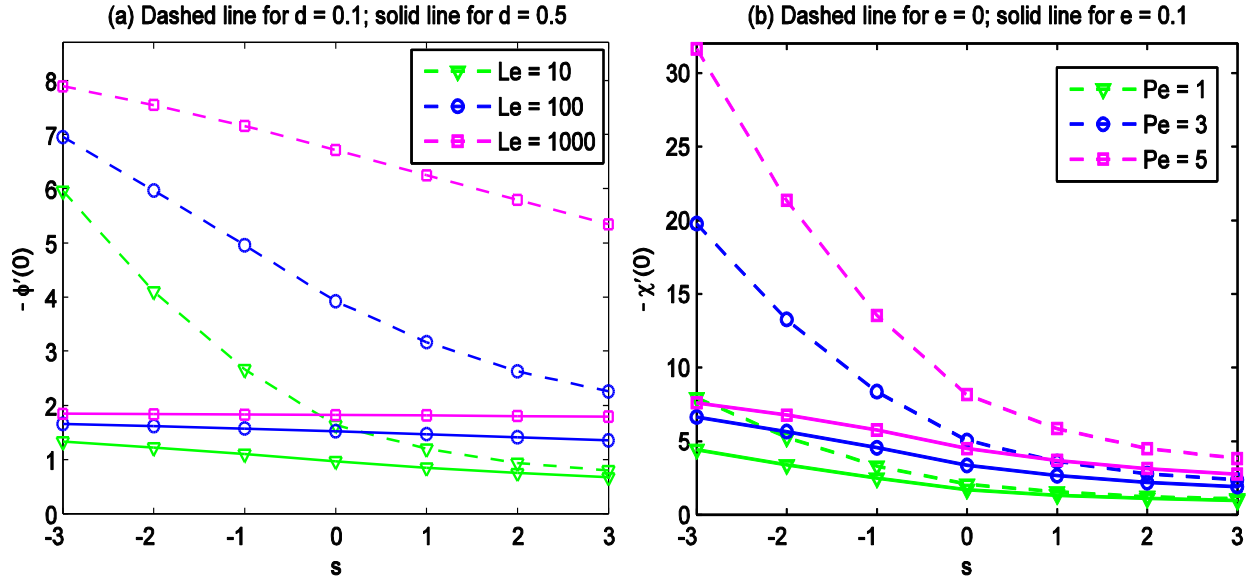
Fig. 13: (a) Effect of the parameters *d* and *Le* on wall mass flux of nanoparicles -$\phi'(0)$ and (b) effect of *e* and *Pe* on wall mass flux of motile microorganism -$\chi'(0)$.

Figs. 2(a)-(b) plot the non-dimensional velocity and temperature profiles for various values of first-order velocity slip *a* and blowing *s*. we observe that dimensionless velocity enhances whilst temperature reduces with the increase in velocity slip for both blowing conditions – injection (s = 1) and suction (s = -1), and the absence of blowing (*s=0*). For the case of suction, nanofluid is drawn inside the boundary through perforations of the sheet. This consequently reduces the momentum which decelerates the flow and increases the velocity boundary-layer thickness. The opposite phenomena occur when injection is induced which enhances the flow and shrinks the velocity boundary-layer thickness. In both cases of injection and suction, the slip decreases progressively with respect to the distance from the wall. However, rising velocity slip leads to a temperature reduction consistently for all locations from the boundary-wall to the free stream. This happens due to enhanced slip that accelerates the flow which cools down the boundary-layer and shrinks the thickness of thermal boundary-layer. Temperature rises with injection but falls with suction. Thermal-boundary layer has the greatest thickness for injection with no-slip at the wall. We notice that at low value of first order momentum slip, a strong velocity shoot arises close to the sheet, which disappears with higher first order slip value. No temperature overshoot is computed for any value of first order velocity slip.

Figs. 3(a)-(b) portray the variation in the profiles of nanoparticle volume-fraction (concentration) and micro-organism concentration with various values of velocity slip *a* and blowing parameter *s*. Both profiles exhibit a monotonic decay from the boundary wall. It can be noticed that nano-particle concentration decreases more rapidly near wall than micro-organism concentration where the latter declines more gradually to zero in the free stream. Both the nano-particle and motile concentrations reduce with greater slip and increase with injection (s=1). A greater spread can be observed in the profiles of nano-particle concentration compared to microorganism concentration. It should be noted that significant similarities as well as differences exist between nano-particles and micro-organisms. The differences may in fact be more beneficial than the similarities. A key problem in nanofluids is mitigation of agglomeration and aggregation, which manifest in clogging phenomena [**2, 3**].

Figs. 4(a)-(b) demonstrate the impact of second-order velocity slip (b) and blowing parameter (suction, no blowing and injection) on the dimensionless velocity and temperature. It can be observed that the dimensionless velocity rises for some distance transverse to the wall with greater second order slip magnitude (b =-5); however further from the wall, the velocity increases weakly i.e. the flow is accelerated with vanishing second order momentum slip (b=0). A velocity shoot near the wall is present in the absence of second order slip whereas it is eliminated when second order slip is present. Temperature however is consistently depressed with greater second order slip magnitude (b= -5) for all cases of blowing, injection and no blowing. Momentum boundary layer thickness at the wall is therefore decreased with greater second order momentum slip close to the wall but the opposite effect is sustained further from the wall. Thermal boundary layer thickness is generally always reduced. The slip parameters whether *momentum, thermal, solutal or micro-organism*, all arise solely in the boundary conditions (32). They do not feature in any of the transformed dimensionless boundary layer equations. The implication for the engineering designer of microbial fuel cells is therefore that significant modifications in boundary layer phenomena are achievable via manipulation of conditions at the wall. These will inevitably also propagate effects further into the main body of the nanofluid and circulation phenomena will be generated. In materials processing, a similar transfer of effects will be felt in the body of the nanofluid sheet via the imposition of wall conditions, but these will progressively diminish with distance from the wall.

Figs. 5(a)-(b) show the influence of second-order velocity slip with blowing parameter (suction, no blowing and injection) on the dimensionless concentration and microorganism. Both nano-particle and microorganism concentrations under second-order velocity slip (b = -5) are observed to be reduced. With second order velocity slip absent the converse behavior is witnessed. The presence of second order slip therefore significantly decreases both nano-particle concentration and micro-organism concentration boundary layer thicknesses. Positive Stefan blowing (injection) always however enhances both nano-particle and micro-organism species concentration magnitudes whereas negative blowing (suction) induces the opposite effect. No overshoots in either concentration function are observed for any value of second order slip or blowing parameter.

Figs. 6(a)-(b) dipict variation in the profiles of dimensionless velocity and temperature with different thermal slips. A higher thermal slip decelerates the flow and suppresses the velocity overshoot adjacent to the boundary. However, a strong reduction in temperature is observed at the wall for higher thermal slip that in turn cools down the boundary layer. Dimensionless temperature gradually vanishes at the free stream. With injection, the flow is mildly accelerated and temperature mildly rises. However, suction decelerates the flow and decreases temperature that leads to a cooler boundary-layer.

The variation in profiles of nano-particle and micro-organism concentrations for different values of thermal slip *c is shown in* **Figs. 7(a)-(b).** A weak *decrease* the nano-particle concentration accompanies an increase in thermal slip whereas the micro-organism concentration weakly increases in magnitudes. For higher thermal slip, diffusion of nano-particles is slightly hindered while propulsion of micro-organisms is slightly improved. Like earlier plots, suction reduces both nano-particle and micro-organism concentrations while injection raises them. Overshoots in both nano-particle and micro-organism concentration are also absent in both figures.

Figs. 8(a)-(b) and 9(a)-(b) present variation in the profiles of dimensionless velocity, temperature, nano-particle and nano-organism concentration for different values of solutal (mass) slip parameter *d*. For higher mass slip at the boundary, nanofluid flow is mildly accelerated and the velocity over-shoot is magnified (Fig 8(a)). Influence of blowing is also remarkable where suction in the absence of mass slip minimizes the velocity, whereas injection with mass slip boosts the velocity. On the other hand, temperature rises with injection and is the minimum with suction with no mass slip

(Fig. 8(b)). With higher mass slip, nano-particle concentration dramatically falls at the vicinity of the wall which is minimized with suction. For injection, nano-particle concentration ascends to the maximum with the absence of mass slip (Fig. 9(a)). A higher mass slip at the wall raises micro-organism concentration, which with injection, elevates to a maximum. In the absence of mass slip, micro-organism concentration distribution with wall suction descends to a minimum. From the figure, we furthermore check that enhanced mass slip improve diffusion of propelling micro-organisms, a feature of some importance in optimized design of biofuel cell designs.

Variation in the profiles of dimensionless velocity, temperature, nano-particle and micro-organism concentrations is demonstrated in **Figs. 10(a)-(b) and 11(a)-(b)** with different microorganism slip parameters e. A higher microorganism slip produces a mild deceleration in the flow and suppresses the velocity overshoot (Fig. 10(a)). Conversely, an increase of microorganism slip slightly increases temperature (Fig.10(b)). With increasing microorganism slip, there is a weak rise in nano-particle concentration (Fig. 11a) whereas the microorganism concentration significantly drops (Fig.11b).

Figs. 12(a)-(b) show the influence of the first- and second-order velocity slips a and b on the dimensionless skin friction factor $f''(0)$ i.e. surface shear stress function, and the influence of thermal slip (c) and Brownian motion parameter (Nb) on heat transfer rate $-\theta'(0)$. With increasing second order slip magnitude a strong reduction in shear stress (Fig. 12a) is induced i.e. the flow is retarded; however with greater first order slip, shear stress generally increases i.e., the flow is accelerated. Shear stress is also as expected observed to be greater for injection ($s>0$) than for suction ($s<0$). Fig. 12(b) shows that heat transfer rate, $-\theta'(0)$ is generally maximized with absence of thermal slip (c=0). Greater magnitudes of heat transfer gradient at the wall are also achieved with higher Brownian motion parameter values ($Nb = 0.1$). Physically a larger Brownian motion number indicates smaller nanoparticle diameters. Heat transfer can be improved in the nanofluid by higher Brownian motion number. On the other hand, lower Brownian motion number implies larger size of nano-particles which leads to reduction of heat transfer.

Figs. 13(a)-(b) exhibit the impacts of mass slip parameter, d and Lewis number, Le on wall mass flux of nanoparticles, $-\phi'(0)$, and also the effect of micro-organism slip, e, and bioconvection Péclet number, Pe on wall mass flux of motile microorganism $-\chi'(0)$. Nanoparticle wall mass flux (Fig. 13(a)) is generally elevated with decreasing solutal slip ($d=0.1$) and higher Lewis number. Solutal slip however exerts a much more significant effect. With strong blowing (injection), nanoparticle wall mass flux is depressed whereas with suction present it is found to be maximized. Fig. 13(b) shows that micro-organism mass flux is substantially increased with bioconvection Peclet number but reduced with increasing micro-organism slip. Peclet number, Pe only exists in the microorganism concentration conservation equation. Note that $Pe = \tilde{b} W_c / D_n$ that uses chemotaxis constant $\tilde{b}$, maximum micro-organism swimming speed W_c and diffusivity of micro-organisms D_n. For higher Pe, Patterns of the motile micro-organism flow dramatically alter. With higher swimming speed of microorganisms i.e., greater Péclet number, microorganisms propel faster which consequently leads to dilution of their concentration. On the contrary, smaller Péclet number produces the reverse effect in that mobility of the micro-organisms reduces which raises their concentration in the nanofluid boundary layer. Injection (s>0) is associated with suppression of micro-organism mass flux while suction (s<0) induces the opposite effect. For blowing effect, the same effect occurs on nano-particle concentration but with smaller magnitude. Finally we note that bioconvection in the present nanofluid regime occurs since nanoparticle concentration is low which does not provide significant increase in the nanofluid viscosity that would inhibit bioconvection (large concentrations of nano-particles can suppress bioconvection and this scenario is not considered here).

8. CONCLUSIONS

In this study, we investigate the influence of multiple boundary slips and blowing on two-dimensional boundary-layer flow over a moving horizontal plate located in a nanofluid comprising of microorganisms. The flow model expressed in terms of partial differential equations was transformed into a system of ODEs by similarity transformation. Then the solution of ODEs with associated boundary conditions was numerically obtained. Test results were verified with the previous results of a model with no-slip and no-blowing condition obtained in the literature, which demonstrated an excellent correlation. Further validation of the generalized model developed was achieved with a Nakamura tri-diagonal finite difference algorithm. A number of interesting results were obtained from the tests. Specifically, the variation of microorganism concentration with various values of Péclet number, blowing, and velocity, tempedrature and microorganism slips is significant. Flow velocity, temperature response, and nanoparticle as well as microorganism concentration are influenced by injection at the wall. Injection was observed to increase micro-organism propulsion and to attain higher flow velocities and to raise the nano-particle concentration. Nanoparticle wall mass flux is boosted with a reduction in mass slip and elevation in Lewis number. Micro-organism mass flux is also remarkably elevated with greater bioconvection Péclet number whereas it is suppressed with increasing micro-organism slip. The present computations are relevant to both near-wall microbial nano-technological biofuel systems (fuel cells) and also the fabrication of bio-nano materials in industrial manufacturing technologies. The current study has overlooked transient and rheological effects, which will be addressed in the future research.

REFERENCES

[1] L. Liu, Aggregation of silica nanoparticles in an aqueous suspension, *AIChE J.* 61 (2015) 2136–2146.

[2] Kaufui V. Wong; Nicholas Perilla; Andrew Paddon, Nanoscience and nanotechnology in solar cells, *ASME J. Energy Resour. Technol.* 136(1) (2013) 014001-014001-9.

[3] G. Nematbakhsh and A. Rahbar-Kelishami, The effect of size and concentration of nanoparticles on the mass transfer coefficients in irregular packed liquid–liquid extraction columns, *Chemical Engineering Communications* 202 (2015) 1493-1501.

[4] M. Bahiraei, S. Mostafa Hosseinalipour and M. Saeedan, Prediction of Nusselt number and friction factor of water-Al_2O_3 nanofluid flow in shell-and-tube heat exchanger with helical baffles, *Chemical Engineering Communications* 202 (2015) 260-268.

[5] F. Su, Y. Deng and H. Ma, Numerical analysis of ammonia bubble absorption in a binary nanofluid, *Chemical Engineering Communications* 202 (2015) 500-507.

[6] E. Zarifi, G. Jahanfarnia, F. Veysi, Subchannel analysis of nanofluids application to VVER-1000 reactor, *Chemical Engineering Research and Design* 91 (2013) 625-632.

[7] Kim, J. K., Akisawa, A., Kashiwagi, T., and Kang, Y. T., Numerical design of ammonia bubble absorber applying binary nanofluids and surfactants, *Int. J. Refrig*. 30 (2007) 1086–1096.

[8] O. Gravel, J. Lauzon-Gauthier, Carl Duchesne, Faïçal Larachi, Inception of vortical coherent structures from spinning magnetic nanoparticles in rotating magnetic fields – New nanofluid microscale mixing tool, *Chemical Engineering J.* 260 (2015) 338-346.

[9] Thadathil S. Sreeremya, Asha Krishnan, A. Peer Mohamed, U.S. Hareesh, Swapankumar Ghosh, *Synthesis and characterization of cerium oxide based nanofluids: An efficient coolant in heat transport applications, Chemical Engineering J.* 255 (2014) 282-289.

[10] Y. Gao, Z. Dai, C. Li and F. Wang, Effects of soot nanoparticles on heat transfer and flow in fire-tube waste heat boiler, *Asia-Pacific J. Chemical Engineering*, 8 (2013) 371–383.

[11] J. Buongiorno, Convective transport in nanofluids, *ASME J. Heat Transfer* 128 (2006) 240–250.

[12] R.K. Tiwari, M.K. Das, Heat transfer augmentation in a two-sided lid-driven differentially heated square cavity utilizing nanofluids, *Int. J. Heat Mass Transf*. 50 (2007) 2002–2018.

[13] M. Kothandapani and J. Prakash, Effects of thermal radiation and chemical reactions on peristaltic flow of a Newtonian nanofluid under inclined magnetic field in a generalized vertical channel using homotopy perturbation method, *Asia-Pacific J. Chemical Engineering* 10 (2015) 259–272.

[14] V.R. Prasad, S. A. Gaffar and O. Anwar Bég, Non-similar computational solutions for free convection boundary-layer flow of a nanofluid from an isothermal sphere in a non-Darcy porous medium, *J. Nanofluids* 4 (2015) 1–11.

[15] M. J. Uddin, O. Anwar Bég, A. Aziz and A. I. M. Ismail, Group analysis of free convection flow of a magnetic nanofluid with chemical reaction, *Math. Prob. Engineering 2015,* Article ID 621503, 11 pp (2015). doi:10.1155/2015/621503.

[16] V. R. Prasad, S. A. Gaffar and O. Anwar Bég, Heat and mass transfer of a nanofluid from a horizontal cylinder to a micropolar fluid, *AIAA J. Thermophysics Heat Transfer,* 29(1) (2015) 127-139.

[17] V. Rajesh, O. Anwar Bég and M. P. Mallesh, Transient nanofluid flow and heat transfer from a moving vertical cylinder in the presence of thermal radiation: Numerical study, *Proc. IMECHE-Part N: J. Nanoengineering and Nanosystems* (2014) 14 pages. DOI: 10.1177/1740349914548712

[18] P. Rana and O. Anwar Bég, Mixed convection flow along an inclined permeable plate: effect of magnetic field, nanolayer conductivity and nanoparticle diameter, *Applied Nanoscience* (2014). 13 pages. DOI 10.1007/s13204-014-0352-z

[19] M.M. Rashidi, S. Abelman, N. Freidooni Mehr, Entropy generation in steady MHD flow due to a rotating porous disk in a nanofluid, *Int. J. Heat Mass Transfer* (2014).

[20] D. Yadav, R. Bhargava, G. S. Agrawal, G. S. Hwang, J. Lee and M. C. Kim, Magneto-convection in a rotating layer of nanofluid, *Asia-Pacific J. Chemical Engineering* 9 (2014) 663–677.

[21] J.R. Platt, Bioconvection patterns in cultures of free swimming organisms, *Science* 133 (1961) 1766-1767.

[22] N.A. Hill and T.J. Pedley, Bioconvection *Fluid Dyn. Res.,* 37 (2005) 1–20.

[23] K. Li, S. Liu and X. Liu, An overview of algae bioethanol production, *Int. J. Energy Research,* 38 (2014) 965–977.

[24] Y. Chisti, Biodiesel from microalgae *Biotechnol. Adv.* 25 (2007) 294–306.

[25] E. Grima, Fernandez J, A. Fernandez F G and Chisti Y, Tubular photobioreactor design for algal cultures, *J. Biotechnol.* 92 (2001) 113–31.

[26] K. G. Satyanarayana, A. B. Mariano and J. V. C. Vargas, A review on microalgae, a versatile source for sustainable energy and materials, *Int. J. Energy Research* 35 (2011) 291–311.

[27] O. P. Roncallo *et al*., Comparison of two different vertical column photobioreactors for the cultivation of nannochloropsis sp., *ASME J. Energy Resour. Technol.* 135 (2012) 011201-011201-7.

[28] E. Le;, C. Park and S. Hiibel, Investigation of the effect of growth from low to high biomass concentration inside a photobioreactor on hydrodynamic properties of scenedesmus obliquus, ASME *J. Energy Resour. Technol.* 2011; 134(1):011801-011801-6

[29] H. Xu, Lie Group analysis of a nanofluid bioconvection flow past a vertical flat surface with an outer power-law stream, *ASME J. Heat Transfer,* 137(4) (2015) 041101.

[30] K. Zaimi, A. Ishak and I. Pop, Stagnation-point flow toward a stretching/shrinking sheet in a nanofluid containing both nanoparticles and gyrotactic microorganisms, *ASME J. Heat Transfer,* 136(4) (2014) 041705.

[31] A.V. Kuznetsov, Nanofluid bioconvection in water-based suspensions containing nanoparticles and oxytactic microorganisms: oscillatory instability, *Nanoscale Research Letters* (2011) 6:100.

[32] O. Anwar Bég, Md. Jashim Uddin and W.A. Khan, Bioconvective non-Newtonian nanofluid transport in porous media containing micro-organisms in a moving free stream, *J. Mechanics Medicine Biology,* 15 (2015) 1550071.1-1550071.20.

[33] A.V. Kuznetsov, Non-oscillatory and oscillatory nanofluid bio-thermal convection in a horizontal layer of finite depth, *Eur. J. Mech B Fluids* 2011, 30(2):156-165

[34] O. Anwar Bég, V.R. Prasad, B. Vasu, Numerical study of mixed bioconvection in porous media saturated with nanofluid and containing oxytactic micro-organisms, *J. Mechanics Medicine Biology,* 13 (2013) 1350067.1-1350067.25.

[35] I. Iliuta, B.P.A. Grandjean, F. Larach Hydrodynamics of trickle-flow reactors: updated slip functions for the slit models, *Chemical Engineering Research and Design* 80 (2002) 195-200.

[36] A. Lawal, Dilhan M. Kalyon, Viscous heating in non-isothermal die flows of viscoplastic fluids with wall slip, *Chemical Engineering Science* 52 (1997) 1323-1337.

[37] E. E. Rosenbaum and S. G. Hatzikiriakos, Wall slip in the capillary flow of molten polymers subject to viscous heating, *AIChE J.* 43 (1997) 598–608.

[38] D. Tripathi, O. Anwar Bég and J. Curiel-Sosa, Homotopy semi-numerical simulation of peristaltic flow of generalized Oldroyd-B fluids with slip effects, *Computer Methods in Biomechanics Biomedical Engineering* 17(4) (2014) 433-442.

[39] M.J. Uddin, M.N. Kabir, Y.M. Alginahi, Lie group analysis and numerical solution of magnetohydrodynamic free convective slip flow of micropolar fluid over a moving plate with heat transfer, Computers & Mathematics with Applications 70(5) (2015) 846-856.

[40] M.J. Uddin, M.N. Kabir, Y. Alginahi, Computational investigation of hydromagnetic thermo-solutal nanofluid slip flow in a Darcian porous medium with zero mass flux boundary condition using stretching group transformations, 18 (2015) 1187-1200.

[41] S. Mankad, P.J. Fryer, A heterogeneous flow model for the effect of slip and flow velocities on food steriliser design**,** *Chemical Engineering Science* 52 (1997) 1835-1843.

[42] C.Y. Wang, Stagnation slip flow and heat transfer on a moving plate, *Chemical Engineering Science* 61 (2006) 7668-7672.

[43] M. Turkyilmazoglu, Exact analytical solutions for heat and mass transfer of MHD slip flow in nanofluids, *Chemical Engineering Science* 84 (2012) 182-187.

[44] M.J. Uddin, O. Anwar Bég and N. Amin, Hydromagnetic transport phenomena from a stretching or shrinking nonlinear nanomaterial sheet with Navier slip and convective heating: A model for bio-nano-materials processing, *J. Magnetism and Magnetic Materials*, 368 (2014) 252-261.

[45] W. Ibrahim and B. Shankar, MHD boundary layer flow and heat transfer of a nanofluid past a permeable stretching sheet with velocity, thermal and solutal slip boundary conditions, *Computers & Fluids* 75 (2013) 1–10.

[46] M.J. Uddin, W.A. Khan, N.S. Amin, g-Jitter mixed convective slip flow of nanofluid past a permeable stretching sheet embedded in a Darcian porous media with variable viscosity, *Plos One,* 9 (6), e99384 (2014).

[47] K. Das, Slip flow and convective heat transfer of nanofluids over a permeable stretching surface, *Computers & Fluids* 64 (2012) 34–42.

[48] Nellis G, Klein S., *Heat Transfer,* Cambridge University Press; pp. E23–5 (2008).

[49] Lienhard IV JH, Lienhard V JH. *A Heat Transfer Textbook*. 3rd ed. Cambridge, Massachusetts, Phlogiston Press, (2005) 662–663.

[50] E Blums, Yu Mikhailov, R Ozols, *Heat and Mass Transfer in MHD Flows*, World Scientific, Singapore (1987).

[51] Abramzon, B. and Sirignano, W. A., Approximate theory of a single droplet vaporization in a convective field: effects of variable properties, Stefan flow and transient liquid heating, *Proc. 2nd ASME-JSME Thermal Engng. Joint Conf, Hawaii, USA, March* (1987).

[52] R.B.Bird, Transport phenomena, *Appl. Mech. Rev*., 55(1), R1-R4 (2002).

[53] Fang, T., & Jing, W., Flow, heat, and species transfer over a stretching plate considering coupled Stefan blowing effects from species transfer, *Comm. Nonlinear Science and Numerical Simulation*, 19(9), (2014) 3086-3097.

[54] Uddin, M.J., Kabir, M.N. and Bég O.Anwar, Computational investigation of Stefan blowing and multiple-slip effects on buoyancy-driven bioconvection nanofluid flow with microorganisms, *International Journal of Heat and Mass Transfer* 95 (2016) 116-130.

[55] Nakamura, S, Iterative finite difference schemes for similar and nonsimilar boundary layer equations, *Advances in Engineering Software,* **21** (1994) 123-130.

[56] A.V. Kuznetsov, D.A. Nield, The Cheng-Minkowycz problem for natural convective boundary layer flow in a porous medium saturated by a nanofluid: A revised model, *Int. J. Heat Mass Transfer*, 65 (2013) 682-685.

[57] Xu, H. and I. Pop., Fully developed mixed convection flow in a horizontal channel filled by a nanofluid containing both nanoparticles and gyrotactic microorganisms, *European Journal of Mechanics-B/Fluids*, 46 (2014): 37-45.

[58] K. Pradhan, S. Samanta, A. Guha, Natural convective boundary layer flow of nanofluids above an isothermal horizontal plate, *ASME J. Heat Transfer,* 136 (2014) 102501.

[59] G Karniadakis, A Beskok, N Aluru, *Microflows and Nanoflows: Fundamentals and Simulation*, Springer, New York (2006).

[60] Beskok, A. and Karniadakis, G.E., Simulation of heat and momentum transfer in complex micro-geometries, *AIAA J. Thermophys. Heat Transfer* 8 (1994) 355-370.

[61] B. J. Cantwell, *Introduction to Symmetry Analysis*, Cambridge University Press (2002).

[62] O. Anwar Bég, J. Zueco, M. Norouzi, M. Davoodi, A. A. Joneidi, Assma F. Elsayed, Network and Nakamura tridiagonal computational simulation of electrically-conducting biopolymer micromorphic transport phenomena, *Computers in Biology and Medicine* **44** (2014) 44–56.

[63] Gorla RSR, Takhar HS and Slaouti A, Magnetohydrodynamic free convection boundary layer flow of a thermomicropolar fluid over a vertical plate, *Int. J. Engineering Science* 36 (1998) 315-327.

[64] Slaouti A, Takhar HS and Nath G, Spin-up and spin-down of a viscous fluid over a heated disk rotating in a vertical plane in the presence of a magnetic field and a buoyancy force, *Acta Mechanica,* 156 (2002) 109-129.

[65] Bég O Anwar, Bég TA, Takhar HS and Raptis A, Mathematical and numerical modeling of non-Newtonian thermo-hydrodynamic flow in non-Darcy porous media, *Int. J. Fluid Mechanics Research,* 31 (2004) 1-12.